Nanoscale

PAPER

View Article Online
View Journal | View Issue

Cite this: *Nanoscale*, 2014, **6**, 1398

Multimodal chemo–magnetic control of self-propelling microbots†

Amit Kumar Singh,[a] Krishna Kanti Dey,[b] Arun Chattopadhyay,[ac] Tapas Kumar Mandal[d] and Dipankar Bandyopadhyay*[ad]

Received 4th October 2013
Accepted 21st October 2013

DOI: 10.1039/c3nr05294j

www.rsc.org/nanoscale

We report a controlled migration of an iron nanoparticle (FeNP) coated polymer micromotor. The otherwise diffusive motion of the motor was meticulously directed through an *in situ* pH-gradient and an external magnetic field. The self-propulsion owing to the asymmetric catalytic decomposition of peroxide fuel was directed through a pH gradient imposed across the motor-surface, while the magnetic field induced an external control on the movement and the speed of the motor. Interestingly, the sole influence of the pH gradient could move the motor as high as ~25 body lengths per second, which was further magnified by the external assistance from the magnetic field. Applying a magnetic field against the pH directed motion helped in the quantitative experimental estimation of the force-field required to arrest the chemotactic migration. The influence of the coupled internal and external fields could halt, steer or reverse the direction the motor inside a microchannel, rotate the motor around a target, and deliver the motor to a cluster of cells. This study showcases a multimodal chemical–magnetic field regulated migration of micro-machines for sensing, transport, and delivery inside a fluidic environment.

Introduction

Recent advances in the fabrication and characterization of small scale devices have inspired the design and development of artificial micro-swimmers,[1–8] mimicking the movements of motor-proteins[9,10] or the motility of microorganisms.[11,12] These synthetic self-propelling objects have important applications in sensing, micro- or nano-fluidic devices, drug delivery,[13] directed self-assembly,[14] and in the design of nano-machinery.[15] In particular, the catalytic decomposition of aqueous hydrogen peroxide (H_2O_2) has been widely employed for the conversion of chemical energy into mechanical motion.[16–21] An electromagnetic field can also be employed to gain external control over the migrations of the nanoscopic objects.[22–27]

Recent studies have revealed that micromotors containing gold (Au) and palladium (Pd) nanoparticles on the surface could undergo pH-directed motion inside a bath of peroxide fuel.[28,29] However, the existing challenge is to gain a multimodal internal–external control on the movements of the synthetic objects to improve their technological usefulness. In this study, we report chemo-magneto-taxis of micro-swimmers in sizes ranging between 30–250 μm, which exhibited directed motion under the coupled influence of an *in situ* pH gradient and an external magnetic field. The self-propelling motion of the motor facilitated by a pH gradient was remotely controlled through an external magnetic field. The external field could meticulously direct the motor during any stage of its migration by steering, halting or even reversing its direction of motion. A host of controlled motions including a reciprocating motion inside a channel and delivery of the motor to a cluster of target animal cells were shown by tuning the internal pH-gradient and the external magnetic field. While the pH-gradient alone could produce a remarkably high speed of ~25 body lengths of the motor per second (~5 mm s^{-1}), the external magnetic field could lead to an explosive increase in the speed when applied in the same direction. The application of the magnetic field against the pH gradient induced migration could decelerate and momentarily stop the motor in both open and confined environments. The minimum magnetic field required to halt a motor undergoing motion due to the pH trigger is arguably the first quantitative and experimental measurement of the magnitude of the force-field of the chemical locomotion. Concisely, this study unveils the pathways to remote-control a self-propelling micro-machine for sensing, transport, and delivery applications.

[a]*Centre for Nanotechnology, Indian Institute of Technology Guwahati, Guwahati – 781039, India. E-mail: dipban@iitg.ernet.in*

[b]*Department of Chemistry, Pennsylvania State University, University Park, Pennsylvania – 16802, USA*

[c]*Department of Chemistry, Indian Institute of Technology Guwahati, Guwahati – 781039, India*

[d]*Department of Chemical Engineering, Indian Institute of Technology Guwahati, Guwahati – 781039, India*

† Electronic supplementary information (ESI) available: Scanning electron microscopy, transmission electron microscopy, X-ray diffraction pattern, vibrating sample magnetometry (VSM) hysteresis loop of freshly prepared FeNP coated micromotor and movies of micromotor motion. See DOI: 10.1039/c3nr05294j

Results and discussion

A recent study showed that a polymeric micromotor decorated with palladium nanoparticles (PdNP) on its surface could undergo a pH directed migration inside a bath of peroxide fuel.[29] The origin of the pH-directed motion of the motor is the coupled influence of the local surface catalytic depletion of aqueous H_2O_2 on the PdNPs together with the global catalytic self-decomposition of H_2O_2 in the bulk of the solution. The present study reveals that replacing the PdNPs with iron nanoparticles (FeNP) can lead to a more versatile motor, which shows a remotely controlled 'external' magnetic field induced migration in addition to the 'internal' pH driven motion.

Fig. 1 shows the experimental setup and the mode of propulsion of the chemo-magneto-taxis reported in this work. The controlled self-propulsion arising from the pH directed motion was experimentally realized by immersing the FeNP coated micromotor inside a bath of aqueous 9.0% (v/v) H_2O_2 solution. The pH gradient was introduced by slowly dripping 0.3 M aqueous sodium hydroxide (NaOH) to the centre of a petridish from a thin cotton thread connected to a reservoir (Fig. 1). The catalytic micromotor responded to this imposed pH gradient when placed a few cm away from the thread and spontaneously migrated towards the thread. The variable magnetic field was applied across the experimental setup with the help of an electromagnet (Fig. 1). A permanent bar magnet of known strength was also used at times to gain control over the motion of the motor.

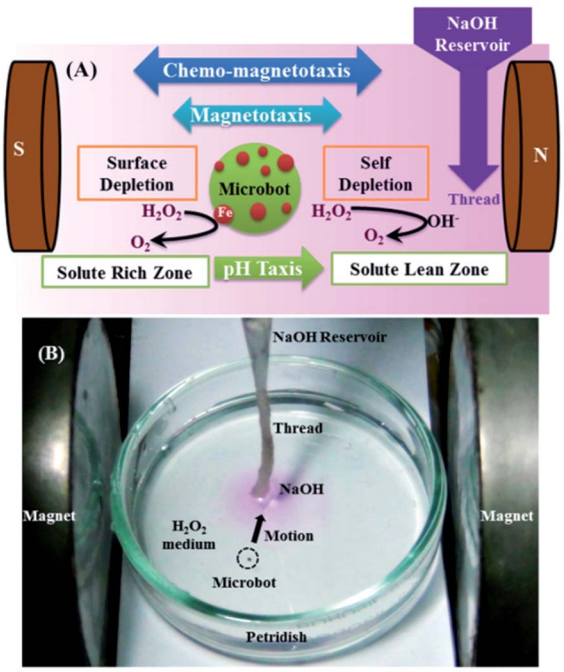

Fig. 1 (A) Schematic illustration of the chemo-magneto-taxis: an iron nanoparticle (FeNP) coated catalytic microbot. The surface decomposition of H_2O_2 catalysed by FeNPs together with self-depletion of H_2O_2 catalysed by alkaline pH results in the migration of the chemo-taxis. The magnetic field driven motion takes place as a consequence of the attractive force between the FeNPs and the applied external magnetic field across the microbot. The coupled motion of the microbot is described using the term "chemo-magneto-taxis", having both internal and external control. (B) Experimental set-up employed for the chemo-magneto-taxis/FeNP coated catalytic microbots. The microbot was placed in a petridish containing aqueous H_2O_2, and a pH gradient was created with the use of a thread connected to an aqueous NaOH reservoir. The advancing alkali front was tracked using a phenolphthalein indicator. The magnetic field was imposed with either the use of an electromagnet or a permanent magnet.

Fig. 2(IA–D) and Video S1 (see ESI†) show that when an FeNP coated micromotor (size ~165 μm) was immersed inside a bath of 9.0% (v/v) aqueous H_2O_2 solution and a pH gradient was imposed, the motor migrated towards the thread. The heterogeneous catalytic decomposition of the H_2O_2 on the FeNPs was clearly visible as the bubbles emanated from the surface of the micromotor. The motion of the micromotor was directed from a region of lower pH to a region of higher pH, which was confirmed by the addition of a trace amount of phenolphthalein in the peroxide bath. The indicator appeared colourless in the acidic region away from the thread, and turned pink in the alkaline region close to the thread. The driving force for the motion was the solute (H_2O_2) pressure imbalance across the micromotor caused by the surface decomposition of peroxide fuel, magnified by the global solute concentration gradient due to the self-depletion of the peroxide fuel in the presence of a pH gradient.[30–34]

The motor migrated towards the thread due to the coupling between the two different types of H_2O_2 depletion: (a) the heterogeneous catalytic surface decomposition of H_2O_2 on the FeNPs, and (b) the homogeneous catalytic decomposition of H_2O_2 resulting from the imposed pH gradient. When the catalytic micromotor was introduced into the peroxide fuel bath, the non-uniformly distributed FeNPs on the surface depleted the peroxide fuel asymmetrically across the surface of the motor. The peroxide–motor interaction through this surface reaction created a *local* imbalance of peroxide concentration across the motor, which led to chaotic motion. The recoil energy arising from the ejection of oxygen bubbles from the motor surface also contributed to the randomness of this movement. The local imbalance of solute concentration due to the surface decomposition of the H_2O_2 was magnified further by the imposed *global* pH gradient. In such a situation, the solute H_2O_2 depleted asymmetrically across the bath as a result of homogeneous catalytic decomposition in presence of alkali. The global depletion of peroxide introduced a larger solute pressure imbalance across the motor, resulting in its acceleration towards the region of higher pH. The experiments also showed that when the motor was further away from the thread (in a region of lower pH), it moved with a uniform speed whereas as it approached the thread, it accelerated significantly before colliding with the thread (in a region of higher pH). Notably, we observed similar catalytic self-propulsion when the motor size was as small as ~30 μm, as shown in Fig. 3C.

In order to confirm that the observed motion was primarily due to the decomposition of the peroxide fuel, we performed a set of control experiments. For example, Video S2 (see ESI†) shows that the motor did not move or discharge any bubbles from the surface in the absence of H_2O_2. In contrast, Video S3 (see ESI†) demonstrates that inside a bath of aqueous H_2O_2, we

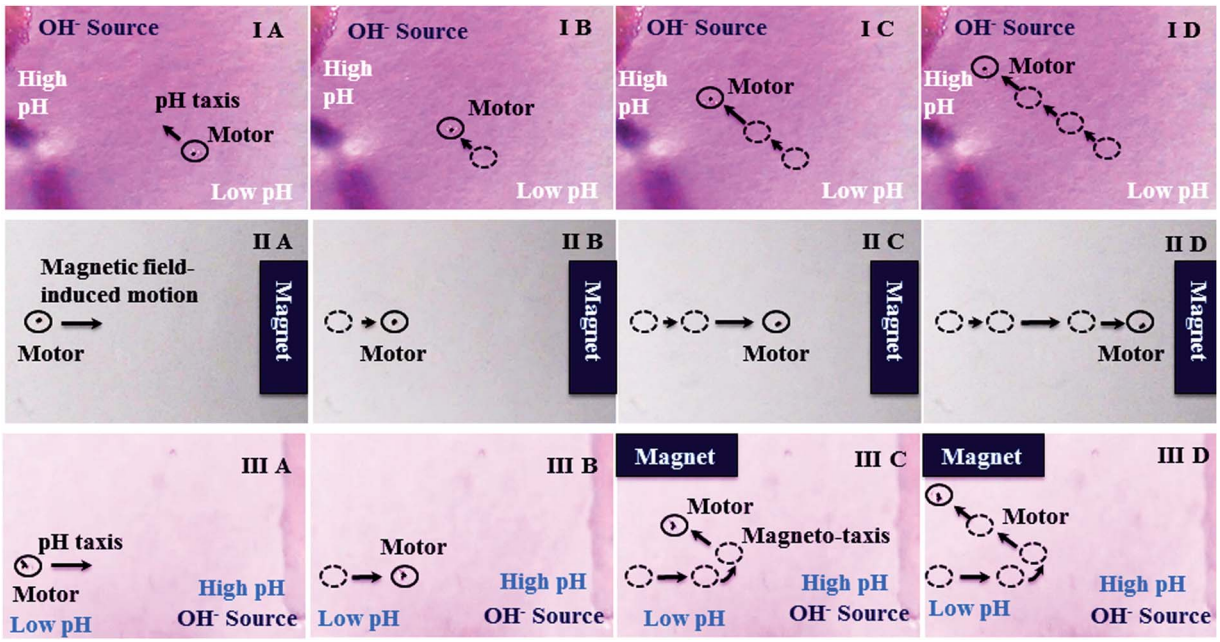

Fig. 2 (IA–D) The chemotactic motion of the motor (~165 μm) towards a thread under a pH gradient. Continuous dripping of aqueous NaOH (0.3 M) into the H_2O_2 bath ensured that the pH was higher in the region near the thread. The advancing alkali front was observed using phenolphthalein indicator in the H_2O_2 bath. (IA–D) The position of the motor at $t = 0$ s, 39 s, 55 s, and 60 s respectively. (IIA–D) The movement towards one of the magnetic poles due to the effect of the applied magnetic field (34 mT) on the motor (~165 μm). (IIA–D) The position of the motor at $t = 0$ s, 10 s, 18 s, and 23 s respectively. (IIIA–D) The coupled chemo-magneto-taxiing of the motor (~165 μm) in which the chemotaxi is seen in (IIIA and B) and the magnetotaxi at 34 mT is shown in (IIIC and D). (IIIA–D) The position of the motor at $t = 0$ s, 35 s, 44 s, and 49 s respectively. In all of the images, the path-history is depicted by broken circular lines while the immediate location is shown by solid circles. The arrowheads show the pathway of the motor.

observed the chaotic motion of the motor as the oxygen bubbles were expelled from the surface. Video S4 (see ESI†) shows that the motor was stationary under the sole influence of a pH gradient, in the absence of H_2O_2. Videos S2–4 (see ESI†) confirm that the decomposition of peroxide was the primary effect giving rise to the self-propulsion of the motor. Importantly,

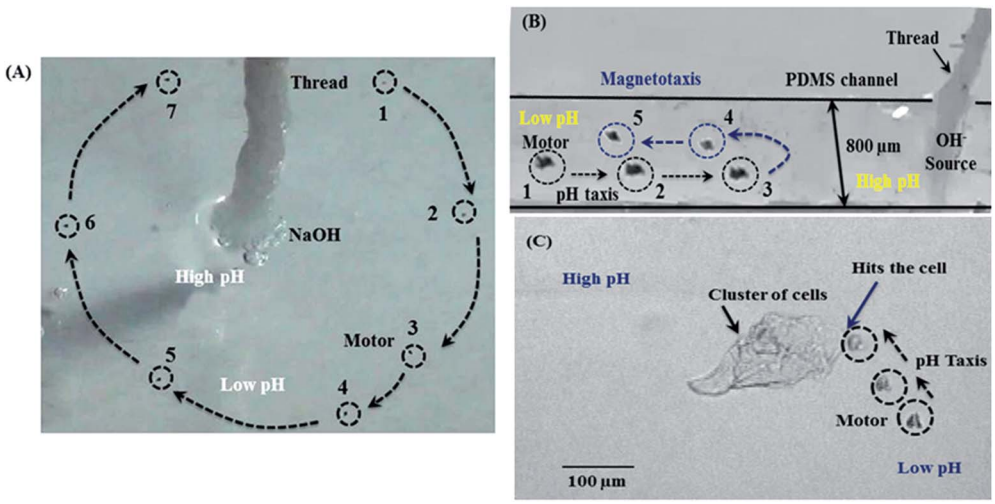

Fig. 3 (A) The magnetic control of a motor (~165 μm) undergoing chemotaxis. The micromotor is moved (from position 1 to 7) around the thread (alkali source) with the assistance of a bar magnet. (B) The reciprocating motion of a motor (~250 μm) in a microchannel with a width of 800 μm, under the coupled influence of the internal pH gradient and the external magnetic field. The directed motion of the motor towards the thread (positions 1 to 3) was generated by the pH gradient (pathway shown by arrows), while motion in the opposite direction to the pH taxis (positions 3 to 5) was generated with the help of an external magnet. (C) A ~30 μm catalytic motor colliding with a cell cluster. The motor migrated towards the cell cluster (~170 μm) due to the imposed pH gradient across the cells. In all of the images the arrows represent the pathway and the broken circular symbols denote the temporal change in the position of the motor.

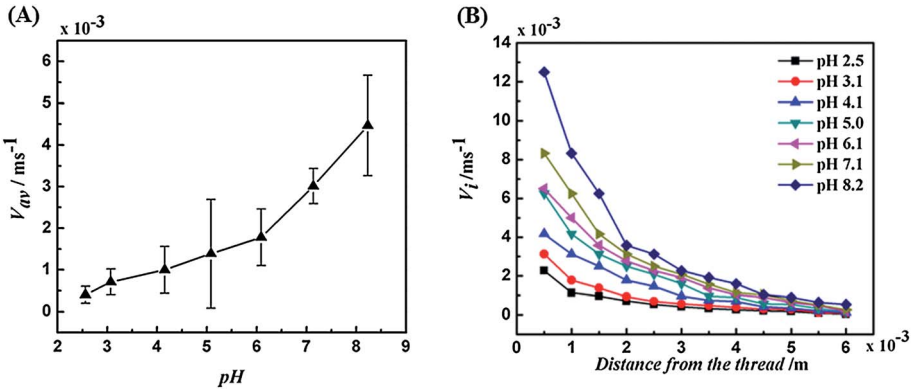

Fig. 4 (A) Variation in the average speed (V_{av}) of a ~180 μm micromotor inside 9% (v/v) H_2O_2 bath when the pH of the bath was varied. (B) Variation in the velocity (V_i) of a ~180 μm micromotor travelling towards the thread (alkali source) at different pH in the 9% (v/v) H_2O_2 bath.

Video S5 (see ESI†) shows that even though the FeNPs were pre-oxidized, the loss of catalytic activity was minimal. Furthermore, in Video S6 (see ESI†), both the alkali source and the bath were maintained at the same pH in order to demonstrate that there was no directed motion, eliminating the possibility that the origin of the motion was due to the mixing of the alkali source and the peroxide bath. Interestingly, in such a situation, since the motor was still catalytically active it showed a 'hopping' motion as the buoyancy of the particle periodically changed while the oxygen bubbles attached or detached from its surface. Video S7 (see ESI†) demonstrates that the motor could be immediately steered in different directions by moving the alkali source to different positions within the peroxide bath. The changes in the source position did not alter the speed of the motor while it changed direction.

The motor was also responsive towards the application of an external magnetic field because of the presence of the FeNPs on its surface. Fig. 2(IIA–D) and Video S8 (see ESI†) show the motion of the motor under the sole influence of an external magnetic field. The induced magnetization of the FeNPs led to the movement of the motor towards the nearest pole of the magnet. Fig. 2(IIIA–D) and Video S9 (see ESI†) show the coupled motion of the micromotor. In this case, in the absence of the magnetic field, initially the motor migrated under the influence of the pH gradient towards the thread. Before reaching the thread, the motor was pulled away in another direction using a

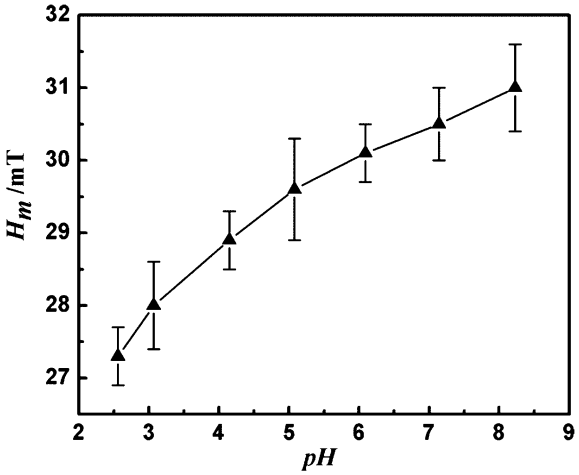

Fig. 6 Variation in the minimum magnetic field (H_m) required to stop a motor (~180 μm) from moving under the influence of a pH gradient, as a function of the pH of the bath.

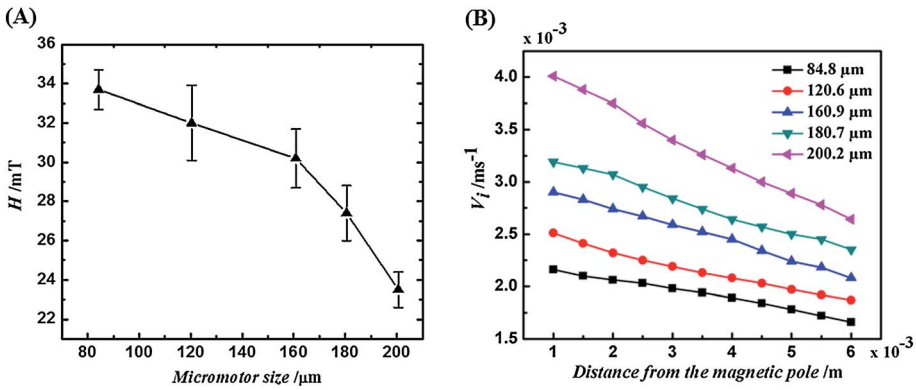

Fig. 5 (A) Variation in the magnetic field strength (H) required to initiate motion of the micromotor with as a function of the motor size (84–200 μm), inside a 9% (v/v) H_2O_2 bath. (B) Variation in the velocity (V_i) of motors of different sizes towards one of the magnetic poles, under the influence of a constant external magnetic field of 35 mT.

permanent magnet. In this process, the directionality of motion of the micromotor under the influence of the internal pH gradient was changed externally by the magnetic field. The control over the movement of the micromotor using the magnet was powerful enough to move it around the thread, as shown in Fig. 3A and Video S10 (see ESI†). Importantly, the motor could resume its migration towards the thread under the influence of the pH gradient once the magnetic influence was withdrawn (not shown in the video or the figure).

Fig. 3B and Video S11 (see ESI)† show another interesting situation where a motor underwent a reciprocating motion inside a PDMS (poly-dimethylsiloxane) channel, under the coupled influence of the internal pH gradient and the external magnetic field. A directed motion of the motor was generated from a region of lower pH towards a region of higher pH, while a motion opposite to the direction of the pH taxis was generated with the help of a permanent magnet. The motion displayed in this situation mimics a controlled movement of an artificial micro-object inside a blood capillary, highlighting the capability of these motors for potential application in sensing, delivery, and transport inside a confined environment. Fig. 3C and Video S12 (see ESI†) show a dummy delivery of motor (~30 μm) into a cluster of cells under the influence of an imposed pH gradient inside a microchannel, in which the source of the pH control is not visible due to high magnification. However, the direction from lower pH to higher pH is indicated in the figure.

The micromotor initially migrated towards the cell cluster (~170 μm) and then collided with it under the influence of the imposed pH gradient. The cells were placed between the thread supplying NaOH and the motor. The motor migrated towards the cell cluster (~170 μm) under the influence of the imposed pH gradient and then hit the cell cluster. It should be noted here, that although we showed a pH gradient mediated delivery of a motor to the cell cluster, the same movements could also be remote-controlled with the use of an external magnetic field. The experiment shown above underlines the potential of the reported motor for the delivery of essential ingredients, such as bio-molecules, drugs, and enzymes, inside living cells.

In order to identify the salient features of the pH induced motion, a series of experiments were performed employing a ~180 μm motor inside a bath of 9.0% (v/v) aqueous H_2O_2 solution, while the pH of the aqueous hydrogen peroxide bath was varied from 2.5 to 8.2. Fig. 4A shows that at lower pH the average speed (V_{av}) attained by the motor was rather low. However, above a pH of 6 the V_{av} increased sharply and we could achieve speeds as high as $\sim 4.46 \times 10^{-3}$ ms^{-1} at pH 8.2, which was equivalent to ~25 body lengths per second. Fig. 4B shows that at constant pH, the local velocity (V_i) of the motor was lower further away from the thread (in a region of lower pH), whereas V_i increased sharply as the motor entered the region of higher pH. Fig. 4B also shows a general increase in V_i at all distances from the thread, with increasing peroxide bath pH.

Experiments were also performed by solely varying the magnetic field across motors of different sizes (84–200 μm) in order to study the effect of the particle size on V_i. Fig. 5A shows that a ~200 μm motor required a minimum magnetic field strength of ~23.5 mT to initiate its movement. In comparison, for a much smaller motor (~84 μm) the minimum magnetic field strength required to initiate motion was much larger, ~33.7 mT. The plots confirmed that a larger amount of FeNPs were deposited on the surface of the bigger motor, which in turn required a smaller magnetic field to initiate movement. The magnetic field strength reported here was measured using a Gaussmeter. Furthermore, when the magnetic field strength was kept constant at 35 mT, it was observed that the bigger motor travelled at a higher speed in comparison to the smaller ones, as shown in Fig. 5B. Together, Fig. 4 and 5 confirmed that the pH gradient and a moderately strong external magnetic field could individually enforce the directed motion of these motors at speeds as high as ~20–25 body lengths per second, which is remarkable. In addition to this we observed that the pH directed motion of the motor could be accelerated significantly with the assistance of a magnetic field.

One of the important findings of this work is a methodology to experimentally measure the magnetic field strength required to resist the pH gradient induced locomotion. For this purpose, a micromotor (size ~180 μm) was initially transported under the influence of pH gradient in a peroxide bath. Subsequently, an external magnetic field was applied in the opposite direction of the motion. Fig. 6 shows the variation in the minimum magnetic field (H_m) required to stop the movement of the motor towards the thread resulting from the pH gradient of the bath. This plot confirms that the force across the motor originating from the pH gradient increased with the pH of the bath, as H_m increased with the same. The magnitude of H_m provides an experimental estimate of the force originating from the differential solute pressure imbalance across the moving motor under the influence of the pH gradient.

Conclusions

The directed self-propulsion of a micromotor under an *in situ* pH gradient was remotely regulated through the application of an external magnetic field, to facilitate locomotion with multimodal internal and external controls. The use of FeNPs on the surface helped in retaining both the magnetic and the pH sensitivity of the motor inside a bath of peroxide fuel. The magnetic field assisted, pH-directed motion exhibited significantly enhanced motor speed, which was otherwise ~25 body length per second under the sole influence of a pH gradient. A host of interesting motions could be achieved when the magnitude and direction of the forces were remotely synchronized. For example, we demonstrated a reciprocating motion towards and away from a target, the delivery of the motor to a target of animal cells, a to and fro motion inside a microchannel, and remotely controlled direction and steering of the motor while it was in motion, including the ability to halt the motor. The control on the directionality of the micromotor together with the control over its speed, employing both the external and internal fields, could make this device a potential candidate for the next generation of self-reliant and remotely controlled micromachines.[35] The attachment of biomolecules, drugs, and cargos with enhanced biocompatibility could open

up the technological viability of these objects for application in imaging, sensing, transport, and drug delivery inside biological environments.[36]

Experimental section

Materials

Amberlite IR 120, hydrochloric acid (HCl), ethanol (C_2H_5OH) (99.9%), hydrogen peroxide (H_2O_2) (50%), sodium hydroxide (NaOH) pellets, potassium permanganate ($KMnO_4$), oxalic acid ($H_2C_2O_4$), boric acid (H_3BO_3), sulfuric acid (H_2SO_4) (98%), 125 mm filter paper (grade 1), acetone ($(CH_3)_2CO$), and methylene blue were obtained from Merck (India). Phenolphthalein, iron(III) chloride hexahydrate ($FeCl_3 \cdot 6H_2O$) and sodium borohydride ($NaBH_4$) were obtained from Sigma-Aldrich (India). For microchannel fabrication, poly-dimethylsiloxane (PDMS) was purchased from Dow Corning, India (SYLGARD® 184 kit). The chemicals above were of analytical grade and used without further purification. The water used in all of the experiments was of Milli-Q grade.

Synthesis of iron nanoparticle (FeNP) coated polymer motors

The method to coat FeNPs onto polymer resins was previously used by a number of research groups.[37,38] In this protocol, 1 g of Amberlite IR 120 Na^+ (cationic polymer resin beads) was crushed into fine particles of dimension 30–250 μm using a pestle and mortar, and cleaned 3–4 times with water before being air-dried on filter paper. The washed beads were suspended in HCl (10 mL, 3.0 M) for 6 h at room temperature (25 °C) for activation. Following this, the beads were washed thoroughly with water to remove excess HCl. Thereafter, the beads were suspended in $FeCl_3 \cdot 6H_2O$ solution (0.54 g dissolved in 10 mL C_2H_5OH) for 6 h at 25 °C before being dries and suspended in 5 mL of water. After this, 5 mL of $NaBH_4$ (0.66 M) was added to the suspension dropwise over 20 minutes with vigorous stirring. The black colour after reduction indicated the formation of FeNPs on the polymer beads. The beads were washed thrice with C_2H_5OH to prevent rapid oxidation, followed by vacuum drying for 2 h at 65 °C. All of the experiments reported were carried out employing freshly prepared FeNP coated motors. Repeated use (2–3 times) of the motors in H_2O_2 could lead to oxidation of the FeNPs. The exact lifetime of the motor depends on the amount of FeNP deposited and the peroxide strength used in the experiments. Importantly, the iron oxides (Fe_2O_3 and Fe_3O_4) were also capable of catalytically decomposing peroxide.[39–41] Hence, the formation of iron oxides did not significantly hinder the chemotaxiing of the motor in a peroxide bath.

Rate constant measurement for H_2O_2 decomposition

It is well known that iron catalyses the decomposition of H_2O_2.[34,42] The concentration of the decomposing H_2O_2 solution in the presence of the FeNPs was analysed by redox titration with $KMnO_4$. The strength of the $KMnO_4$ was standardized by using 0.2 N oxalic acid as the primary standard. Initially, a 6 mL aliquot of 9% (v/v) H_2O_2 was prepared at a particular pH, which as adjusted using 0.3 M NaOH solution. A collection of 450 crushed beads were suspended in this solution. We prepared a number of such solutions and employed them one by one for the estimation of the rate of decomposition of H_2O_2 at different time intervals. For a particular time interval, 0.3 g of H_3BO_3 was added to arrest the decomposition of H_2O_2 before an aliquot of 300 μL was withdrawn and added to a solution of 10 mL 0.2 N H_2SO_4. Following this, the sample was titrated against standard 0.2 N $KMnO_4$ in which a permanent weak pink coloration indicated the end point. The rate constant (k) for the peroxide decomposition was determined graphically from the change in H_2O_2 concentration with time. The linearity of the plot confirmed that the H_2O_2 decomposition followed first-order kinetics. This process was repeated for all of the pH values in presence of catalytic and non-catalytic beads. The catalytic rate constant (k_{cat}) was measured alongside the non-catalytic rate constant ($k_{non\text{-}cat}$) for the H_2O_2 decomposition in the presence of the same number of beads. The net rate constant (k_{net}) was assumed to be the difference between k_{cat} and $k_{non\text{-}cat}$, which is the contribution of the FeNPs in the H_2O_2 decomposition. The effective rate constant (k_{eff}) of a single bead was obtained by dividing the net rate of decomposition (k_{net}) by the number of particles.[29]

Velocity measurements under the influence of a pH gradient

A micromotor (size ~180 μm) was suspended in 4 mL of 9% (v/v) aqueous H_2O_2 inside a petridish (3 cm diameter). The alkali gradient was introduced at the centre of the petridish *via* a thread connected to a reservoir containing 0.3 M NaOH. The petridish was placed on a paper-grid (0.5 × 0.5 mm dimension) to measure the displacement of the motor. The pH gradient was confirmed by the addition of phenolphthalein (~0.15 g in 50 mL) to the H_2O_2 solution. The velocity of the motor was studied at different pH values. The speed of the motor was measured at a position sufficiently far away from the thread to minimize the effect of acceleration towards the thread. The velocity was estimated by measuring the particle displacement from a starting point 6 mm away from the thread to an end point near the thread, and dividing the displacement by time taken for the particle to travel that distance. For a particular pH, the speed was measured separately for three different micromotors of similar size and the mean is reported as the average speed (V_{av}) of the particle.[24] The velocity of the motor (V_i) was calculated after every 0.5 mm displacement of the motor per unit time towards the thread under the influence of the pH gradient.

Velocity measurements under the influence of an external magnetic field

Micromotors (size ~84 μm to 200 μm) were suspended in a petridish filled with 4 mL of 9% (v/v) aqueous H_2O_2 solution. The petridish was placed on a paper-grid (0.5 × 0.5 mm dimension) to measure the displacement of the motors. A constant magnetic field of 35 mT was applied across the petridish with the use of an electromagnet. The velocity of the motor (V_i) was calculated after every 0.5 mm displacement of the motor per unit time towards one of the poles of the magnet. The critical field required to initiate the motion was estimated

by placing the motor (size ~84 μm to 200 μm) in a petridish filled with 4 mL 9% (v/v) H_2O_2 solution and then increasing the magnetic field steadily until the motion was observed. For a motor of a particular size, independent experiments were performed with three different motors to obtain the mean value and the error bars.

Minimum magnetic field (H_m) measurement

Micromotors with a size of ~180 μm were suspended in a petridish filled with 4 mL of 9% (v/v) aqueous H_2O_2, and the alkali gradient was imposed *via* a thread connected to the 0.3 M NaOH reservoir. Once the motor moving under the influence of the pH gradient, the magnetic field was applied against the direction of motion. The H_m reported is the minimum magnetic field required to pull the particle against the pH directed motion. The experiment was repeated for pH 2.5 to 8.2 and the effective magnetic force required to pull the particle in the opposite direction to the pH gradient were measured using a Gaussmeter. The mean values and error bars were calculated from three independent experiments using different motors ~180 μm in size.

PDMS microchannel fabrication

A template (mould) of desired dimensions was cut from thin aluminum sheets using a 2.5 kW carbon dioxide Laser Cutting Machine (LVD Company). The surface of the template was cleaned with ethanol and acetone. The curing agent and the PDMS were mixed thoroughly for 30 min in a 1 : 10 ratio, avoiding the formation of air bubbles while mixing. Following this, the mixture was poured at the edges of the mould before placing it in an oven in air at 60 °C for 40 minutes. The cast was removed carefully from the mould with the help of acetone. The dimensions of the microchannel (800 × 400 μm) were determined under a microscope.

Micromotor motion inside a microchannel

A micromotor with a size of ~250 μm was suspended in 9% (v/v) aqueous H_2O_2 inside the microchannel. The alkali gradient was imparted at one end of the channel *via* a thread connected to an alkali reservoir. The microparticle started moving towards the thread under the influence of the imposed pH gradient. The motor was then pulled away from the thread with the assistance of a permanent magnet.

Micromotor travelling towards and hitting animal cells

Human epithelial cheek cells were collected by gently swabbing the cheek portion inside the mouth with a cotton bud. Then the isolated cells were suspended in a 1.5 mL micro-centrifuge tube containing 2 mL of water. 2 μL of methylene blue was added into the tube to stain the cells. After gently shaking the tube, it was kept for 20 minutes in ambient conditions. The typical size of the isolated single cheek cell varied from 60 to 85 μm. A 10 μL aliquot of the cell solution was dispensed into a microchannel filled with 9% (v/v) aqueous H_2O_2. Following this, a motor with a size of ~30 μm was suspended and the pH gradient was introduced *via* a thread connected to a NaOH reservoir. The cells were always positioned between the motor and the thread. The motor hitting a cluster of cells with a size of ~170 μm was observed under a microscope.

Characterization techniques

Scanning electron microscopy (SEM, JEOL JSM 6360, operated at 30 kV) and transmission electron microscopy (TEM, JEOL JEM 2100, operated at 200 kV) were used to examine the particle morphologies. The samples were dried and placed on carbon tape adhered to a stub before being gold-sputtered for SEM analysis. For TEM analysis, the samples were dispersed in ethanol and then drop-casted onto a carbon coated Cu-grid and dried at room temperature. The formations of nanoparticles over the polymer resins were further confirmed by X-ray diffraction (XRD, Bruker AXS Advance D8 diffractometer, Cu K_α source, X-ray wavelength 1.54 Å). The magnetization curve was determined by vibrating sample magnetometer (VSM, Lakeshore GMW magnetic systems 3474-140). The pH of the solutions was measured with a CyberScan Scan pH 510 meter (Eutech Instruments). The motion of the moving micromotor was recorded with a Sony Cybershot DSC-HX100V digital camera (Sony Corp., Japan). The micromotors of varying sizes were picked under a Leica DM 2500 upright microscope. The electromagnet Model EMU-50V with a constant current power supply unit (DPS – 50) and a bar magnet with dimensions of 10.2 cm × 1.7 cm and a magnetic field gradient of 1 mT mm^{-1} were used to apply the magnetic fields in various experiments, and the applied magnetic fields were measured using a Digital Gaussmeter Model DGM-102 (purchased from SES instruments, India).

Acknowledgements

We thank DST Nano-Mission program, Grant no. SR/NM/NS-1109/2012(C), Government of India, for the financial aids. We also thank Prof. Perumal Alagarsamy (Department of Physics, IIT Guwahati) for the measurements through the VSM facility. The support from Central Instrumentation Facility, IIT Guwahati for characterization facilities is also gratefully acknowledged.

Notes and references

1 W. F. Paxton, K. C. Kistler, C. C. Olmeda, A. Sen, S. K. St. Angelo, Y. Cao, T. E. Mallouk, P. E. Lammert and V. H. Crespi, *J. Am. Chem. Soc.*, 2004, **126**, 13424.
2 U. K. Demirok, R. Laocharoensuk, K. M. Manesh and J. Wang, *Angew. Chem., Int. Ed.*, 2008, **47**, 9349.
3 G. Huang, J. Wang and Y. Mei, *J. Mater. Chem.*, 2012, **22**, 6519.
4 S. J. Ebbens and J. R. Howse, *Soft Matter*, 2010, **6**, 726.
5 L. F. Valadares, Y. Tao, N. S. Zacharia, V. Kitaev, F. Galembeck, R. Kapral and G. A. Ozin, *Small*, 2010, **6**, 565.
6 J. Li, G. Huang, M. Ye, M. Li, R. Liu and Y. Mei, *Nanoscale*, 2011, **3**, 5083.
7 Z. Liu, J. Li, J. Wang, G. Huang, R. Liu and Y. Mei, *Nanoscale*, 2013, **5**, 1345.

8 Y. Mei, A. A. Solovev, S. Sanchez and O. G. Schmidt, *Chem. Soc. Rev.*, 2011, **40**, 2109.
9 R. Mallik and S. P. Gross, *Curr. Biol.*, 2004, **14**, 971.
10 M. Schliwa and G. Woehlke, *Nature*, 2003, **422**, 759.
11 H. C. Berg, *Phys. Today*, 2000, **53**, 24.
12 T. Mirkovic, N. S. Zacharia, G. D. Scholes and G. A. Ozin, *ACS Nano*, 2010, **4**, 1782.
13 W. Gao, D. Kagan, O. S. Pak, C. Clawson, S. Campuzano, E. Chuluun-Erdene, E. Shipton, E. Fullerton, L. Zhang, E. Lauga and J. Wang, *Small*, 2012, **8**, 460.
14 R. F. Ismagilov, A. Schwartz, N. Bowden and G. M. Whitesides, *Angew. Chem., Int. Ed.*, 2002, **41**, 652.
15 Y. Wang, S. Fei, Y. Byun, P. E. Lammert, V. H. Crespi, A. Sen and T. E. Mallouk, *J. Am. Chem. Soc.*, 2009, **131**, 9926.
16 A. Agrawal, K. K. Dey, A. Paul, S. Basu and A. Chattopadhyay, *J. Phys. Chem. C*, 2008, **112**, 2797.
17 S. Sundararajan, P. E. Lammert, A. Zudans, V. Crespi and A. Sen, *Nano Lett.*, 2008, **8**, 1271.
18 L. Qin, M. J. Banholzer, X. Xu, L. Huang and C. A. Mirkin, *J. Am. Chem. Soc.*, 2007, **129**, 14870.
19 J. G. Gibbs and Y. P. Zhao, *Small*, 2009, **5**, 2304.
20 J. Wang and K. M. Manesh, *Small*, 2010, **6**, 338.
21 L. Baraban, S. M. Harazim, S. Sanchez and O. G. Schmidt, *Angew. Chem., Int. Ed.*, 2013, **52**, 5552.
22 T. R. Kline, W. F. Paxton, T. E. Mallouk and A. Sen, *Angew. Chem., Int. Ed.*, 2005, **44**, 744.
23 J. Burdick, R. Laocharoensuk, P. M. Wheat, J. D. Posner and J. Wang, *J. Am. Chem. Soc.*, 2008, **130**, 8164.
24 L. Baraban, D. Makarov, O. G. Schmidt, G. Cuniberti, P. Leiderer and A. Erbe, *Nanoscale*, 2013, **5**, 1332.
25 K. K. Dey, K. K. Senapati, P. Phukan, S. Basu and A. Chattopadhyay, *J. Phys. Chem. C*, 2011, **115**, 12708.
26 G. Zhao and M. Pumera, *Langmuir*, 2013, **29**, 7411.
27 G. Zhao, S. Sanchez, O. G. Schmidt and M. Pumera, *Chem. Commun.*, 2012, **48**, 10090.
28 K. K. Dey, B. R. Panda, A. Paul, S. Basu and A. Chattopadhyay, *J. Colloid Interface Sci.*, 2010, **348**, 335.
29 K. K. Dey, S. Bhandari, D. Bandyopadhyay, S. Basu and A. Chattopadhyay, *Small*, 2013, **9**, 1916.
30 U. M. Córdova-Figueroa and J. F. Brady, *Phys. Rev. Lett.*, 2008, **100**, 158303.
31 J. F. Brady, *J. Fluid Mech.*, 2011, **667**, 216.
32 J. L. Anderson, *Annu. Rev. Fluid Mech.*, 1989, **21**, 61.
33 J. L. Moran and J. D. Posner, *J. Fluid Mech.*, 2011, **680**, 31.
34 J. Weiss, *Adv. Catal.*, 1952, **4**, 343.
35 A. A. Solovev, S. Sanchez, M. Pumera, Y. F. Mei and O. G. Schmidt, *Adv. Funct. Mater.*, 2010, **20**, 2430.
36 D. Patra, S. Sengupta, W. Duan, H. Zhang, R. Pavlick and A. Sen, *Nanoscale*, 2013, **5**, 1273.
37 H. Shu, M. Chang, C. Chen and P. Chen, *J. Hazard. Mater.*, 2010, **184**, 499.
38 Z. Zongshan, L. Jingfu, T. Chao, Z. Qunfang, H. Jingtian and J. Guibin, *Sci. China: Chem.*, 2008, **51**, 186.
39 S. Lin and M. D. Gurol, *Environ. Sci. Technol.*, 1998, **32**, 1417.
40 M. Hermanek, R. Zboril, I. Medrik, J. Pechousek and C. Gregor, *J. Am. Chem. Soc.*, 2007, **129**, 10929.
41 M. A. Nejad and M. Jonsson, *J. Nucl. Mater.*, 2004, **334**, 28.
42 J. Abbot and D. G. Brown, *Int. J. Chem. Kinet.*, 1990, **22**, 963.